Available online at www.sciencedirect.com
SCIENCE DIRECT®
Surface Science 566–568 (2004) 221–225
SURFACE SCIENCE
www.elsevier.com/locate/susc

Surface morphology of antiferromagnetic $Fe_{50}Mn_{50}$ layers on Cu(0 0 1)

W. Kuch *, L.I. Chelaru, J. Kirschner

Max-Planck-Institut für Mikrostrukturphysik, Weinberg 2, D-06120 Halle, Germany

Available online 2 June 2004

Abstract

The growth and the morphology of ultrathin $Fe_{50}Mn_{50}$ alloy films, deposited by thermal co-evaporation of Fe and Mn on Cu(0 0 1) at room temperature are studied by scanning tunneling microscopy (STM). A high density of small islands of single and double atomic height is nucleated during the initial stages of growth of $Fe_{50}Mn_{50}$ on Cu(0 0 1). The film growth proceeds further in a nearly perfect layer-by-layer mode. Topographic STM images corresponding to $Fe_{50}Mn_{50}$ film thicknesses above 10 atomic monolayers reveal atomically flat terraces with islands or holes of monoatomic height (≈0.18 nm). In addition, a fine structure with an apparent corrugation height of about 0.05 nm is recognized. Scanning tunneling spectroscopy measurements prove the spectroscopic origin of this corrugation. It is attributed to local concentration differences of the constituents of the chemically disordered $Fe_{50}Mn_{50}$ alloy.

Keywords: Scanning tunneling microscopy; Surface structure, morphology, roughness, and topography; Single crystal epitaxy; Scanning tunneling spectroscopies; Iron; Manganese

1. Introduction

The details of the interface between a ferromagnetic (FM) and an antiferromagnetic (AF) thin film strongly influence the phenomena resulting from the magnetic coupling between FM and AF layers. Despite the great interest in the FM/AF interface coupling and the huge amount of work dedicated to its investigation, a full understanding of the observed phenomena is still elusive (see, for example, Refs. [1,2] and references therein). This is in part due to the incomplete characterization of the interface in the sputtered polycrystalline bilayers that are typically used. To study FM–AF coupling at well defined interfaces, epitaxial single crystalline layers are required. Because of the low lattice mismatch (0.4%), $Fe_{50}Mn_{50}$ films [3] (FeMn in the following) on a Cu(0 0 1) single crystal are ideal candidates for such investigations. Epitaxial, virtually unstrained FeMn films can be grown in a layer-by-layer mode by thermal deposition on Cu(0 0 1) at room temperature [4]. This provides the opportunity to study the magnetic properties of an AF/FM system in single crystalline FeMn/Co and Co/FeMn bilayers on Cu(0 0 1) [4–7].

Here we present a scanning tunneling microscopy (STM) study of the surface morphology of ultrathin FeMn layers on Cu(0 0 1). The FeMn layer in Co/FeMn and FeMn/Co bilayers on

* Corresponding author. Tel.: +49-345-5582615; fax: +49-345-5511223.
E-mail address: kuch@mpi-halle.de (W. Kuch).

0039-6028/$ - see front matter © 2004 Elsevier B.V. All rights reserved.
doi:10.1016/j.susc.2004.05.046

Cu(0 0 1) is known to exhibit antiferromagnetism at room temperature for thicknesses above 10 atomic monolayers (ML) [4,5]. We focus first on the initial stages of growth of FeMn on Cu(0 0 1), before we present results for FeMn layers with thicknesses above 10 ML. The results provide valuable information about the details of the FM–AF interface that is formed upon Co deposition on top of FeMn/Cu(0 0 1).

2. Experiment

The experiments were performed in a multichamber ultrahigh vacuum system with a base pressure below 10^{-8} Pa. The disk-shaped Cu(0 0 1) single crystal was cleaned by cycles of 1 keV argon ion bombardment at 300 K and subsequent annealing at 873 K for 15 min. The surface exhibited a sharp (1×1) low energy electron diffraction pattern coinciding with large atomically flat terraces observed by STM, typically larger than 100 nm. No contaminations were detectable by Auger electron spectroscopy (AES).

Fe_xMn_{1-x} films of equiatomic composition ($x = 0.50 \pm 0.02$) were deposited at room temperature by co-evaporation from two different evaporation sources, in which Fe and Mn rods of 99.995% and 99.5% purity, respectively, were heated by electron-bombardment. Typical evaporation rates were 1 ML per minute. The composition of the FeMn films was estimated from the evaporation rates of the separate sources, and cross-checked by AES peak ratios. No indications for segregation of Cu into or on top of the alloy layers were found. It can not be excluded on the basis of the AES data, however, that some material exchange between Cu and FeMn may occur directly at the FeMn/Cu interface. The thickness of the films was determined by reflection high-energy electron diffraction (RHEED), which showed the same layer-by-layer oscillations as observed previously by medium energy electron diffraction (MEED) [4], and by analysis of STM images with an accuracy within 0.1 ML.

STM measurements were carried out with a commercial room temperature ultrahigh vacuum STM [8], operated in constant current mode of operation using polycrystalline PtIr tips. Spectroscopic information was gained by measuring current–voltage (I–U) curves under open feedback conditions.

3. Results and discussion

Fig. 1(a) presents an STM image after deposition of 1.3 ML FeMn on Cu(0 0 1). The morphology of the surface is dominated by relatively small islands in the second layer, with an average

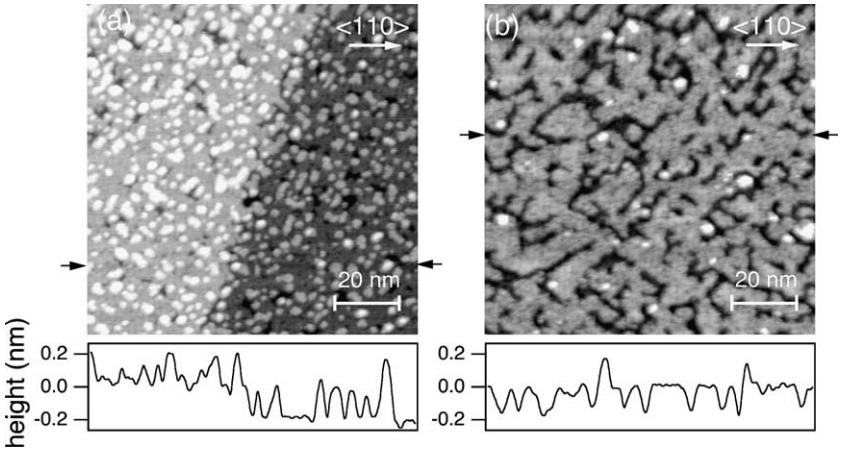

Fig. 1. STM constant current images. (a) 1.3 ML FeMn/Cu(0 0 1) ($U_{bias} = 0.2$ V, $I = 0.1$ nA); (b) 2.7 ML FeMn/Cu(0 0 1) ($U_{bias} = 0.5$ V, $I = 0.2$ nA). Line profiles taken along horizontal lines at positions marked by arrows are shown at the bottom of each image.

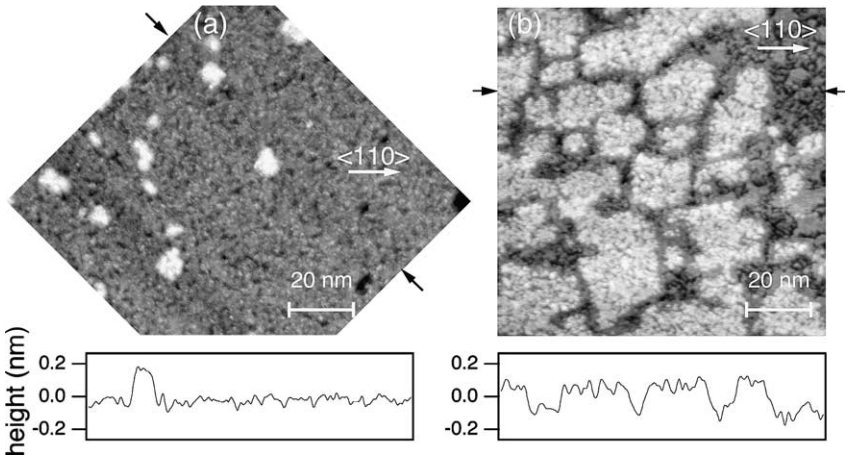

Fig. 2. STM constant current images. (a) 10.0 ML FeMn/Cu(0 0 1); (b) 11.7 ML FeMn/Cu(0 0 1) ($U_{bias} = 0.5$ V, $I = 0.2$ nA). Line profiles taken along lines marked by arrows outside the images are shown at the bottom of each image.

density of 44×10^3 μm^{-2}, on top of a nearly closed first layer. Mean island sizes are typically of the order of 2–5 nm diameter. Both, islands of single and double atomic height, are observed. A monoatomic step of the substrate is recognized in the center of the image. Holes in the first layer, at which the substrate surface is exposed, are found at several positions (e.g., black spots at the right hand side of the image). The linescan presented at the bottom of the image shows the height profile along a horizontal line indicated by arrows outside the image. Closer inspection of the line profile reveals that the apparent height of the islands does not always exactly correspond to pseudomorphic single or double atomic step height (0.18 nm). Moreover, the apparent height of some of the islands changes with bias voltage. This may be an indication for intermixing of Fe and Mn with Cu atoms in these initial stages of growth.

Fig. 1(b) shows the surface of a 2.7 ML FeMn film. At this coverage, coalescence of the third layer is complete. Some islands have already nucleated in the fourth layer, which are recognized as small white spots. Black grooves correspond to exposed area of the second layer. The linescan presented below the image indicates a more regular height distribution, corresponding to pseudomorphic monoatomic steps of 0.18 nm height.

FeMn film thicknesses above 10 ML, which are interesting for studies of FM–AF interactions, are presented in Fig. 2. Fig. 2(a) shows the topographic image of 10.0 ML FeMn/Cu(0 0 1), Fig. 2(b) the topographic image of 11.7 ML FeMn/Cu(0 0 1). The STM images confirm the nearly perfect layer-by-layer growth mode as already concluded from the presence of MEED and RHEED oscillations during growth. Island sizes are significantly larger than in the initial stages of growth. Only a few islands are seen at 10.0 ML FeMn thickness on top of a nearly complete 10th layer (Fig. 2(a)). Some black spots in the rightmost part of the image represent holes in the 10th layer. In Fig. 2(b), coalescence of the 12th layer is still incomplete at 70% coverage. Islands of about 20 nm width are separated by grooves of single atomic depth. While the direction of these trenches is preferentially along $\langle 1\,1\,0 \rangle$ directions, the trenches in Fig. 1(b) are preferentially oriented along $\langle 1\,0\,0 \rangle$ directions. Different anisotropy of atom diffusion in the initial and later stages of growth could be the reason behind that.

Within the atomically flat regions of Fig. 2(a) and (b), some finer corrugated structure is recognized in the topographic images. Consecutive scans at the same sample position confirm the reproducibility of this corrugation. Linescans of the images, taken at the positions indicated by arrows, are presented below each image. They confirm that the islands and grooves discussed above indeed correspond to monoatomic steps of

pseudomorphic FeMn layers, i.e., exhibit 0.18 nm step height. In addition to these steps, a corrugation of about 0.05 nm apparent height is observed within the islands and terraces.

To further investigate the origin of this corrugation, scanning tunneling spectroscopy measurements were performed. Fig. 3(a) and (b) show current map images of the 11.7 ML FeMn film for positive and negative bias voltage, respectively. It is evident from comparison of the two images that the observed features change contrast when changing the bias voltage. Fig. 3(c) shows a constant-current topographic image at the same position. A meandering horizontal terrace edge of monoatomic step height is seen within the imaged area. It is not visible in the current maps (a) and (b), since they were recorded at constant tip height. In addition to that step edge, the same fine corrugation as in Fig. 2 is also seen here. Fig. 3(d) shows I–U curves of the areas labelled A and B in panels (a)–(c), corresponding to darker and brighter regions in panel (a), respectively. Qualitatively, in region A the tunneling I–U curve shows a plateau within −0.2 and +0.5 eV, followed by a linear increase in the current. At negative voltages the tunneling curve exhibits a strong exponential increase corresponding to a peak in the differential conductivity $\mathrm{d}I/\mathrm{d}U$, shown in the inset of panel (d), at −0.5 eV. When the tip is located over region B, the tunneling current shows a linear dependence for positive voltages, while for negative bias a peak in the differential conductivity $\mathrm{d}I/\mathrm{d}U$ at −0.3 eV is observed.

Comparing the topographic image, Fig. 3(c), and the current map images (a) and (b), it is seen that most features related to the 0.05 nm corrugation in Fig. 3(c) are related to spectroscopic features. To facilitate this comparison, we present

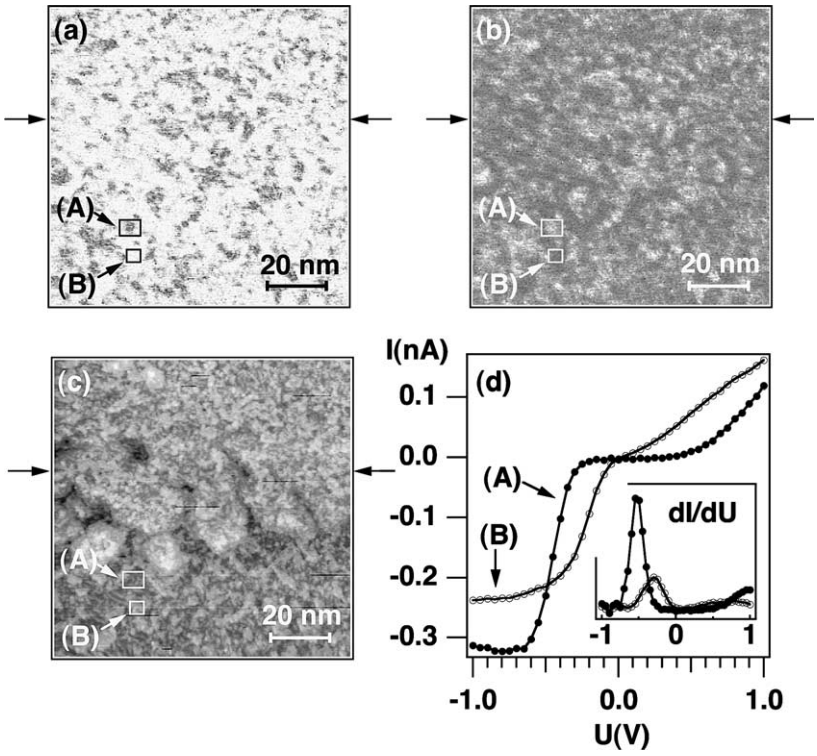

Fig. 3. Comparison of current map and topographical images at the same position of 11.7 ML FeMn/Cu(0 0 1). (a) Current map image at 0.4 V; (b) current map image at −0.15 V; (c) constant current image ($U_{\mathrm{bias}} = 0.5$ V, $I = 0.2$ nA); (d) tunneling I–U curves averaged over the areas labelled A and B in panels (a)–(c). Inset: derivative of the I–U curves showing the differential conductivity.

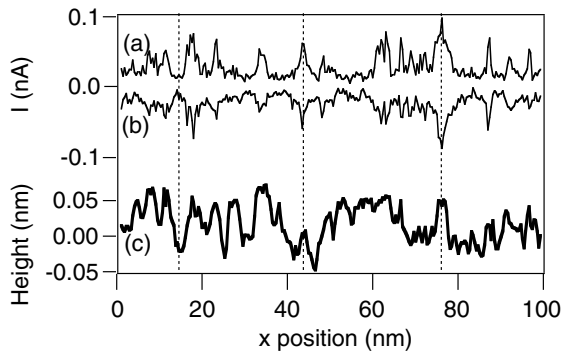

Fig. 4. Line profiles taken at identical positions along horizontal lines in Fig. 3(a)–(c), as marked there by arrows. Vertical dotted lines highlight the correlation between spectroscopic features in curves (a) and (b), and features in the topographical line profile (c) at three positions.

in Fig. 4 horizontal linescans of the data of panels (a)–(c) of Fig. 3, taken at identical positions marked by arrows. It is seen that many of the features observed in the constant current image are indeed related to spectroscopic features of Fig. 3(a) and (b). We conclude therefore that the observed fine corrugation of a fraction of a monoatomic step height is of spectroscopic origin. Considering the compositionally disordered chemical structure of the alloy films, it is conceivable to relate these spectroscopic differences to local differences in the concentration of the two constituents. At the moment we are not able to correlate the two different I–U curves as displayed in Fig. 3(d) to either Fe or Mn rich regions at the surface of the films. A quantitative interpretation of the presented data would require knowledge of the electronic structure of the sample. Further systematic studies controlling the average composition x of Fe_xMn_{1-x} films, supported by theoretical electronic structure calculations, are necessary to elucidate these details. It should be mentioned that these I–U curves represent the two extreme cases observed in the images, while the contrast in both the current maps and the topographic images varies with a smaller apparent amplitude on a lengthscale of about 1 nm, which is probably resolution limited. The larger areas of a few nm extension of preferential bright or dark contrast seen in Fig. 3(a) and (b) may in addition indicate some chemical phase separation, which could be driven by local strain or electronic properties.

4. Conclusion

Because of the epitaxial layer-by-layer growth on Cu(0 0 1), antiferromagnetic $Fe_{50}Mn_{50}$ ultrathin films are well suited for studies of the interface interaction between antiferromagnetic and ferromagnetic layers. The roughness at the surface of $Fe_{50}Mn_{50}$/Cu(0 0 1) is confined to islands and holes of single atomic step height even for FeMn thicknesses above 10 ML, the thickness range of interest for the study of magnetic AF/FM coupling. Evidence for lateral concentration differences of the constituents of the chemically disordered FeMn alloy on the nm scale comes from scanning tunneling spectroscopy. The presented data provide valuable information for the interpretation of magnetic studies of FeMn/Co bilayers on Cu(0 0 1) [4–7].

Acknowledgements

We would like to thank J. Barthel, G. Kroder, and H.L. Meyerheim for help during the experiments. Stimulating discussions with W. Wulfhekel, U. Schlickum, W. Pan, and D. Sander are gratefully acknowledged.

References

[1] J. Nvogués, I.K. Schuller, J. Magn. Magn. Mater. 192 (1999) 203.
[2] R.L. Stamps, J. Phys. D: Appl. Phys. 33 (2000) R247.
[3] Y. Endoh, Y. Ishikawa, J. Phys. Soc. Jpn. 30 (1971) 1614.
[4] F. Offi, W. Kuch, J. Kirschner, Phys. Rev. B 66 (2002) 064419.
[5] W. Kuch, F. Offi, L.I. Chelaru, M. Kotsugi, K. Fukumoto, J. Kirschner, Phys. Rev. B 65 (2002) 140408.
[6] F. Offi, W. Kuch, L.I. Chelaru, K. Fukumoto, M. Kotsugi, J. Kirschner, Phys. Rev. B 67 (2003) 094419.
[7] F. Offi, W. Kuch, L.I. Chelaru, M. Kotsugi, J. Kirschner, J. Magn. Magn. Mater. 261 (2003) L1.
[8] Omicron NanoTechnology.